ON THE VARIABILITY OF THE PULSED FRACTION IN X-RAY PULSING BINARIES

A. C. Williams, K.M.V. Apparao*, and M. C. Weisskopf

Space Science Laboratory
NASA Marshall Space Flight Center
Huntsville, Alabama 35812

RECEIVED
SEP 15 1987
NASA STI FACILITY
NASA/MSFC
NASA S.T.I. LIBRARY

*Space Physics Group
TATA Institute of Fundamental Research
Bombay, India

(NASA-TM-89665) ON THE VARIABILITY OF THE PULSED FRACTION IN X-RAY PULSING BINARIES (NASA) 30 p Avail: NTIS

N88-70089

Unclas
00/89 0114149

Abstract

We have calculated how the pulsed fraction varies as a function of optical depth for a variety of geometries of the distribution of matter about an X-ray pulsar. These calculations were then applied to observations of the X-ray sources Her X-1, Cyg X-3, and A0538-66. The Hercules results indicate a strong correlation between the pulsed fraction and intensity and are entirely consistent with an interpretation whereby variations in both parameters are due to the intervention of varying amounts of matter between the pulsar and the observer. A similar conclusion can be applied to the A0538-66 observations. In the case of Cyg X-3, we performed a search for periodic pulsations on subsecond timescales. The absence of any detected pulsation, together with our calculations, are shown to be entirely consistent with the assumption of a spherical shell of gas around the neutron star. We suggest that studies of the pulsed fraction as a function of intensity compliment studies of spectral variations and can be used as an additional diagnostic tool in order to understand the nature of the distribution of matter surrounding the pulsating X-ray sources.

Subject Headings: pulsars-stars: neturon-X-rays: binaries-scattering: Thompson

I. Introduction

X-radiation passing through matter is scattered. Scattering removes some radiation from the line of sight while bringing radiation from other directions into the line of sight. Scattering has the effect of altering the pulsed fraction. In this paper we consider Thompson scattering from a cold gas and study the variation of the pulsed fraction with optical depth. In Section II we present calculations for three different geometries: a cylindrical shell, a spherical shell, and a uniform sphere, each surrounding an X-ray pulsar. In Section III, we apply the results of our calculations to the X-ray sources Her X-1, Cyg X-3, and A0538-66, where we believe the three different configurations are relevant. In Section IV, we present a summary and our conclusions.

II. Calculational Method and Approximations

a. General Formalism and Approximations

We consider an X-ray pulsar as an isotropically emitting point source of X-rays, blinking on and off with pulse period T. This approximation simplifies calculations and is valid if the size of the pulsar and cT are both very much less than the characteristic dimension of the surrounding medium. In the applications which we consider both these conditions appear to be satisfied.

b. General Formalism

We define t_0 as the instant of time at which a distant observer would detect the first photons from an isotropically emitting pulsed source. Let F be the fraction of photons that have passed through the surrounding scattering medium and are detected by the distant observer. We define f_n (n = 0, 1, 2,...) as the fraction of emitted photons which undergo exactly n scatterings before being detected. Let $P_n(t)dt$ be the corresponding fraction detected between the times t and t + dt. Thus

$$f_n = \int_{t_0}^{\infty} P_n(t)dt \qquad (1)$$

$$F = \sum_{n=0}^{\infty} f_n \ . \qquad (2)$$

The observed temporal profile from this single delta function pulse, q(t)dt, is then simply

$$g(t)dt = \frac{\sum_{n=0}^{\infty} P_n(t)dt}{F} . \qquad (3)$$

Since we have to consider many pulses, the equilibrium pulse profile will involve the integrated contribution from previous pulses. We define G(t)dt as the number of photons detected between t and t+dt, where

$$G(t)dt = \sum_{j=0}^{\infty} g(t+jT)dt = \frac{\sum_{j=0}^{\infty}\sum_{n=0}^{\infty} P_n(t+jT)dt}{F} . \qquad (4)$$

We note that G(t) is normalized to one when integrated over a single pulse period

We define the pulsed fraction, F_p, (as any observer would) utilizing the minimum in the observed pulse profile as indicative of the "unpulsed" component. In this case, since the underlying input is a delta function spike the minimum is always at the end of a pulse period, i.e. at $t_o + T$. Thus

$$F_p = 1 - TG(t_o+T) = 1 - \frac{T}{F}\sum_{n=0}^{\infty}\sum_{j=0}^{\infty} P_n(t_o+T+jT) . \qquad (5)$$

In principle the knowledge of $P_n(t)$ for all n determines F_p. In practice, however, these functions are difficult to calculate analytically for $n > 1$ (see e.g., Williams et al. 1984), and therefore we will further restrict ourselves to small optical depths for electron scattering ($\tau \lesssim 2$). This condition allows one to accurately estimate F_p by only calculating $P_1(t)$.

In order to obtain an expression for F_p we proceed as

follows. First we rewrite equation (4), as

$$G(t) = G^{(1)}(t) + R(t) \tag{6}$$

where

$$G^{(1)}(t) \sum_{j=0}^{\infty} \sum_{n=0}^{1} P_n(t+jT), \tag{7}$$

and R(t) includes the remaining terms. Similarly we can write

$$F_p = F_p^{(1)} - \frac{T}{F} R(t_o+T) \tag{8}$$

where $F_p^{(1)}$ is the pulsed fraction considering only unscattered and singly scattered photons. $F_p^{(1)}$ could serve as a first approximation to F_p, and it certainly is an upper limit. A much better approximation (and also an upper limit) follows from the fact that

$$R(t_o+T) > \frac{(F-f_o-f_1)}{f_1} G^{(1)}(t_o-T) \ . \tag{9}$$

since photons scattered more than once have a higher probability of being detected at the end of a pulse. It follows then that

$$F_p^{(2)} < F_p^{(1)} - \frac{T}{F} \frac{(F-f_o-f_1)}{f_1} G^{(1)}(t_o+T)$$

$$= 1 - \frac{T}{F} G^{(1)}(t_o+T) \left[1+(F-f_o-f_1)/f_1\right] \ . \tag{10}$$

c. Spherical Geometry

In this section we calculate $P_0(t)$ and $P_1(t)$ in order to estimate F_0 for the case where the pulsar is at the origin of a spherical shell of inner radius R_1 and outer radius R_2. We exploit the spherical symmetry and consider all the photons emerging from the scattering medium. Thus we get $F = 1$ and the fraction of unscattered photons is

$$f_0 = e^{-\tau_0} \tag{11}$$

where τ_0 is the optical "thickness" of the spherical shell. In this case

$$P_0^{(t)} = e^{-\tau_0} \delta(t-t_0) \tag{12}$$

where t_0 is the time it takes for an unscattered photon to reach the observer.

To obtain $P_1(t)$, we use the scattering kernel, which describes single Thomson scattering (assuming an unpolarized source). The distribution of photons which travel a distance s, scatter by an angle θ, and then emerge from the medium before scattering again, is

$$K(s, \mu)ds d\mu = \frac{3}{8}(1+\mu^2)\, e^{-\tau(s,\mu)}\, \kappa\rho ds d\mu \ . \tag{13}$$

Here $\mu = \cos\theta$, $\tau(s,\mu)$ is the optical thickness through which the above photon will traverse, κ is the mass absorption coefficient

and ρ is the mass density. The total optical thickness of the medium is

$$\tau_o = \alpha\rho(R_2-R_1) \ . \tag{14}$$

The difference in the arrival time, t_d, of a single scattered photon and an unscattered photon is (see also Figure 1)

$$t_d = t-t_o = \frac{s}{c}(1-\mu) \ . \tag{15}$$

where c is the speed of light. It is convenient to define

$$t' \equiv \frac{t_d c}{R_2} = \frac{s(1-\mu)}{R_2} \ . \tag{16}$$

To obtain the distribution, $P_1(t')$, we change variables from s and μ to b and t' where

$$b = \mu(1 - s/R_2) \ . \tag{17}$$

with these new variables,

$$P_1(t') = \int_{b_1(t')}^{b_2(t')} \frac{\tau_2}{2(1+\tau/\tau_2)} \left[1+(t'+b+1)\left[(t'+b-1)^2+4t'\right]^{-1/2}\right] H(\tau,\mu)db$$

$$0 \leq t' \leq 2 \tag{18}$$

where

$$b_1(t') = \begin{cases} 1+\tau_1/\tau_2 - t'(1+\tau_2/\tau_1) , & 0 \leq t \leq 2\,\tau_1/\tau_2 \\ -(t'+2)/2 , & 2\tau_1/\tau_2 \leq t \leq 2 , \end{cases} \tag{19}$$

$$b_2(t') = 2(1-t') , \tag{20}$$

$$\tau_1 = \tau_o\, R_1/(R_2-R_1) , \tag{21}$$

$$\tau_2 = \tau_o\, R_2/(R_2-R_1) , \tag{22}$$

$$\tau = \frac{\tau_2}{2}\left\{t'+b-1 + \left[(t'+b-1)^2+4t'\right]^{1/2}\right\} , \tag{23}$$

$$H(t',b) = \frac{3}{3}\,(1+u^2)\, e^{-q(\tau,u)} , \tag{24}$$

$$u = b/(1+\tau/\tau_2) , \tag{25}$$

and

$$\tau(1-u) + \left[\tau_2^2 - \tau^2(1-u^2)\right]^{1/2} - \tau_1$$

$$q(\tau,u) = \begin{cases} \text{(for } u > 0 \text{ or } \tau > \tau_1\,(1-u^2)^{-1/2} \\ \tau(1-u) - \left[\tau_2^2 - \tau^2(1-u^2)\right]^{1/2} - \left[\tau_1^2 - \tau^2(1-u^2)\right]^{1/2} - \tau_1 \\ \text{(for } u < 0 \text{ and } \tau < \tau_1\,(1-u^2)^{-1/2} . \end{cases} \tag{26}$$

The fraction f_1 can then be calculated from either of

$$f_1 = \int_0^2 P_1(t')\, dt' \tag{27}$$

or

$$f_1 = \int_{\tau_1}^{\tau_2} \int_{-1}^{1} H(\tau, \mu)\, d\mu d\tau \ . \qquad (28)$$

Using Equations (7) and (10), the pulsed fraction can be written as

$$F_p^{(2)} = 1 - \frac{T'(1-f_o)}{f_1} \sum_{j=0}^{jmax} P_1(T'+jT') \qquad (29)$$

where T' is the dimensionless period ($T' = TC/R_2$) and jmax is defined by

$$jmax = Int(2/T' - 1) \ . \qquad (30)$$

Figures 2 and 3 show $F_p^{(2)}$ as a fraction of the optical thickness for two particular examples.

4. Cylindrical Geometry

We made no attempt to perform analytic calculations for cylindrical geometries of the scattering medium. Rather, Monte Carlo calculations were performed, first for the spherical geometry to validate the software and do calculations described in Section Ib, and then to provide the results for this case. The simulation took into account all orders of scattering and tabulated the emerging photons according to their direction. Typical results for photons traveling essentially radially outward from the axis of the cylinder are listed in Table 2.

e. Generalization

The pulsed fraction that we have calculated is that relevant for a point source emitting a pulse of radiation which is a delta function in time. The intrinsic temporal distribution, of course, is not a delta function. If one is given the actual distribution $I_o(t)$ of the source, then the pulse shape of the observed radiation can be obtained by convolving our results with the distribution $I_o(t)$.

This convolution must be applied to the emerging photons probability distribution, $P_n(t)$. The new distribution will be given by

$$P_n'(t) = \int_{-\infty}^{\infty} P_n(t-t') \, I_o(t') \, dt' \, . \qquad (31)$$

The time, t_o, of section IIb will now have to represent the time that the pulse turns on. That is, $I_o(t) = 0$ for $t < t_o$. In addition, the source will turn off at some specific time later which we denote by t_1. Hence $[((t_1-t_o)/T) \times 100\%]$ is just the intrinsic duty cycle. Eq. (31) can then be written as

$$P_n'(t) = \int_{t_o}^{t_1} P_n(t-t') \, I_o(t') \, dt' \, . \qquad (32)$$

It follows then that all of the previous formalism will be the same, provided that $P_n(t)$ is everywhere replaced by $P_n'(t)$. In particular, the pulsed fraction of eq. (5) becomes

$$F_p = 1 - \frac{T}{F} \sum_{n=0}^{\infty} \sum_{j=0}^{\infty} P_n' \, (t_o + T + jT) \, . \qquad (33)$$

The effect of carrying out the integration in eq. (32) would be to smear $P_n(t)$ into a wider temporal distribution $P_n'(t)$. If the intrinsic duty cycle of the pulses are small, then there will not be much smearing, and our delta function results are directly applicable. If the smearing is significant, however, then it is evident that this will cause the second term in eq. (33) to be larger than it would be for the delta function case. This, in turn, means that the actual pulsed fraction is smaller than we have calculated.

Hence, if one is only interested in a reasonable upper limit to the pulsed fraction, as we are, then the calculations we have done are appropriate. On the other hand, if one wishes to extend our work to obtain a more precise calculation of the pulsed fraction, then eq. (32) must be used.

Another point worth discussing relates to cases where the intrinsic pulsed fraction is less than 100%. In this case, the observed pulsed fraction will be given by

$$F_p^{(OBS)} = F_p \, F_p^{(INT)}$$

where F_p is the pulsed fraction we have calculated in equation (33), and $F_p^{(INT)}$ is the pulsed fraction intrinsic to the source.

III. Applications and Results

In this section we now apply our calculations as approximations to the configurations of matter near the X-ray sources Her X-1 (cylindrical shell), Cyg X-3 (spherical shell), and A0538-66 (uniform spherical cloud). For each source, we have supplemented published measurements of the pulsed fraction with additional results obtained by us through an analysis of observations of these sources by the Monitor Proportional Counter (MPC) (Gaillardetz et al., 1978; Grindlay et al., 1980; Weisskopf et al., 1981) aboard the Einstein observatory.

a. Her X-1

Her X-1 displays variations with periods of 1.24s, 1.7d, and 35 d. The first period is due to the rotation of the neutron star and the second due to binary motion. The 35 day variation is attributed to the precession period of an accretion disk around the neutron star (see Boynton, Deeter, and Crosa, 1980). The precession is suggested to bring the outer regions (rim) of the disk between the neutron star and the observer; the consequent attenuation causes the observed change in intensity. However, doubts have been cast as to the reality of this mechanism (Kondo et al., 1983; Naranan et al., 1985).

Her X-1 also displays dips in its X-ray intensity lasting about 4 hours, with the intensity being reduced by a factor of about 5 (Giacconi et al., 1973). The dips occur in every orbital cycle, starting just before the eclipse and marching away from the time of eclipse with the progression of

orbital cycles. These dips have been suggested to be due to the surge of matter injected by the primary into the outer regions of the accretion disk in a periodic fashion (Crosa and Boynton, 1980). Hence, the increased amount of matter at the rim coming in between the X-ray source and the observer is the cause of the dip. Recently, it was found that the X-ray intensity in these dips is not constant, but displays flare like activity (Ogelman, et al., 1984; Dil Vrtilek et al., 1984). The origin of this activity is maybe wave-like disturbances, induced by the surge of matter injected at the edge of the accretion disk. The troughs in this wave will lead to reduced amount of matter in the line of sight of the observer, and consequently, less attenuation and enhanced X-ray emission.

If the 35 day variability and the large increases in intensity in the dips are due to differing amounts of matter coming between the X-ray source and the observer, then this should lead to corresponding changes in the pulsed fraction. The variation of the pulsed fraction during 35 day cycles of Her X-1 has been given by Joss et al. (1978). These are plotted as a function of intensity in Figure 4. The high intensity results indicate an "intrinsic" pulsed fraction of about 0.55. If the reduction in intensity below 60 units (see Figure 4) is attributed to absorption by cold matter, and we associate the high intensity results with $\tau \sim 0$, then making some assumptions about the geometry and density of the scattering medium, we can predict the reduction in pulsed fraction.

We assume that the outer regions of the disc, can be approximated by a cylindrical shell of uniform density at a distance of 10^{11} cm and a thickness of the same value (see Hayakawa, 1981). The expected pulsed fraction for τ of 1 and 1.5 and two different values of the height of the cylinder were given in Table 1. Associating the high intensity state with $\tau = 0$ implies a τ of 1 to reduce the intensity from 60 to 23. The corresponding reduction in pulsed fraction, for $h/R_2 = 1$, implies a change in the pulsed fraction from 0.55 to 0.32, which is to be compared with the observed value of 0.2 ± 0.08. The agreement is satisfactory considering all the uncertainties and assumptions.

We have also analyzed an observation of Her X-1 on JD2443949 with the MPC. These data were taken during preeclipse dips. The measured pulsed fractions are also shown in Figure 4 and labelled as H (flaring) and L (quiescent). Again, we see good agreement between theory and observation.

Hence, the correlation of the pulsed fraction with intensity is consistent with that expected due to Thomson scattering by cold matter and supports models which suggest that the changes in X-ray intensity of Her X-1, for both the 35 day cycle and the dips, occur due to intervention of matter between the X-ray source and the observer.

b. Cyg X-3

The X-ray source Cyg X-3 has an X-ray luminosity of about 10^{38} ergs s^{-1}. The source has been observed in the gamma ray, X-ray, infrared, and radio bands but not in the visible.

The infrared (Mason et al., 1976) and X-ray emission (Parisignault et al., 1972; Elsner et al., 1980 and references therein) show a 4.8 hr variation which is attributed to the orbital motion of a neutron star around a companion. It was suggested (Milgrom, 1976; Milgrom and Pines, 1978; and Bignami, Maraschi, and Treves, 1977) that the neutron star is a fast rotator with a period of the order of a few tens of milliseconds, somewhat similar to the pulsar in the Crab Nebula. The 4.8 hr periodicity is then explained by postulating a spherical shell of gas around the neutron star system (Milgrom, 1976; and Milgrom and Pines, 1978). The shell is suggested to be at a distance of $\sim 10^{12}$ cm with a thickness of $\sim 1.3 \times 10^{11}$ cm and a density $\rho \sim 10^{13}$ H-atoms cm^{-3}. No observations of X-ray pulsation from Cyg X-3 have been reported.

We have used MPC observations of Cyg X-3 to search for pulsations. The observations were made on JD2443989. We performed a Fast Fourier Transform analysis on the data. The period range searched was 0.003 s to 0.33 s. No periodicity was found and the (90%, 90%) confidence upper limit (see Leahy et al., 1983) to the pulsed fraction is 0.07. In the case of periods less than 0.01 s, binary motion could have smeared the pulses. To take this effect into account, we assumed a 4.8 hr binary period, the epoch given by Elsner et al. (1980), and we corrected the arrival times for Doppler shifts using 1.5, 3, 5, and 7 light seconds as the projected radius of a circular orbit. We then reperformed the Fast Fourier Transform analysis. Again, we found no evidence for pulsations.

We suggest that the lack of observation of a pulsation is due to the presence of the gas shell. The line of sight integrated gas density towards Cyg X-3 is $\sim 10^{24}$ H-atoms cm^{-2}, (see Milgrom, 1976) which corresponds, for Thomson scattering, to an optical thickness of $\tau \sim 0.7$. It this case, (see Figure 2), the pulsed fraction is reduced by a factor of 2.3. This, combined with the upper limit on the pulsed fraction given above, indicates that the pulsar in Cyg X-3 could only have been observed if the intrinsic pulsed fraction was greater than 0.16. By comparison, the pulsar 0531+21 in the Crab Nebula whose period is 33 milliseconds, shows $F_p \sim 0.15$ for X-ray energies greater than 10 kev, decreasing to about 0.03 at about 1 kev. The MPC observations cover the bandwidth from 1.1 to 22 keV. Thus if the pulsar in Cyg X-3 were to be observed in X-rays one requires extremely high sensitivities as may be obtained in the future with X-ray Timing Explorer or the Japanese satellite ASTRO-C.

Recently, gamma rays of 1000 GeV have been observed from Cyg X-3 showing a 12.6 ms periodicity (Chadwick et al., 1985). If these observations are confirmed, a search for X-ray pulsations with very high sensitivity may be fruitful.

c. A0538-66

The X-ray source A0538-66 is located in the Large Magellanic Cloud. It has active and inactive periods. When it is active, the X-ray emission occurs in flares lasting several hours to days. The flares recur every 16.6 days (Skinner et al.,

1980). The X-ray emission displays a 69 milliseconds periodicity (Skinner et al., 1982). The 16.6 day periodicity is attributed to orbital period of a neutron star in an eccentric orbit orbiting a Be star. The X-ray emission occurs when the neutron star is near periastron (Charles et al., 1983; Apparao, 1985). Charles et al. (1983) suggest that a cloud of gas is formed near periastron due to the tidal pull of the neutron star and the accretion of this gas onto the neutron star results in X-ray emission. Apparao (1985) uses the fact that Be stars are known to eject rings of gas in the equatorial plane in a quasi-periodic fashion and suggests that the X-ray emission occurs when the neutron star passes through this ring. In either case the X-radiation emitted by the neutron star passes through the residual matter in the ring or cloud along the line of sight of the observer. The value of τ depends on the position of the neutron star.

Skinner et al. (1982) reported two observations of A0538-66. Pulsations were detected in the first observation in 1980 December when the average flux was ~ 40 MPC counts s^{-1}. The pulsed fraction was $F_p \approx 0.2$. The power law spectral index was -1.6. Pulsations were not observed during the second observation in 1981 February, which was shorter, when the average flux was ~ 10 MPC counts s^{-1}. The power law spectral index was -0.6 indicating a harder spectrum. The (90, 90%) confidence upper limit (Leahy et al., 1983) for the pulsed fraction was $F_p \leq 0.19$. The decrease in intensity for the second observation and the hardening of the spectrum indicate absorption by matter and

that the optical depth was larger than in the first observation. Proceeding as for Her X-1, we assume that the first observations correspond to $\tau \sim 0$. On this assumption then, the indicated increase in τ is ~ 1.2 and, using the curve in Fig. 2, the predicted reduction in F_p is by a factor of 3, not inconsistent with our observation. Future observations of the change of the pulsed fraction during flaring of A0538-66 could provide further information as to the structure of matter near the periastron of the neutron star.

IV. Summary

We have calculated the variation expected in the observed pulsed fractions of x-radiation from X-ray pulsars when matter of three different geometries--cylindrical shell, spherical shell, and uniform shell--is introduced between the source and the observer. The results have been applied to Her X-1, Cyg X-3, and A0538-66. In the case of Her X-1, the variation of the pulsed fraction during the 35 day cycle indicates that this quasi-periodic variation is due to intervention of matter between Her X-1 and the observer. This is consistent with the outer regions of the accretion disk acting as the screen. We have measured the pulsed fraction during the flares in the intensity dips of Her X-1 and again find that the increase in intensity during flares is consistent with lessening of the column density of matter along the line of sight. The suggestion that a surge from the periodic injection of matter at the outer rim of the disc is the cause of the dips is also consistent with the observed variation.

We have attempted to detect pulsations in the X-ray emission from Cyg X-3 using the data from the Einstein Observatory. We do not detect pulsations for periods between 0.003 to 0.33 sec and place an upper limit of 7% to the pulsed fraction. Using our calculations we conclude if a pulsar of the Crab Nebula type exists in Cyg X-3, the pulsations will be reduced to a very low amplitude by a spherical shell of gas of the type postulated to account for the 4.8 hr X-ray variation and the infrared radiation.

These results were shown to be consistent with current models wherein the X-rays are produced when the neutron star passes through a ring or cloud of gas at closest approach to the Be companion.

We feel that preliminary calculations and their successful, semi-quantitative application to known systems have demonstrated the usefulness of the study of variation in the pulsed fraction as a new diagnostic tool for understanding the physical conditions in and around the pulsing X-ray binaries. This tool should be utilized to complement and extend the information which can be gleaned from purely spectroscopic studies. Future work in this are calls for more realistic calculations which consider not only the details of accretion discs, etc., but also take into account the detailed nature of the X-ray production mechanism and the conditions near the surface of the neutron star. Coupled with spectroscopic and polarization measurements, measurements of the pulsed fraction can lead to a deeper understanding of the complex intensity variations observed.

Table 1. Monte Carlo calculations of the pulsed fraction from a source within a cylindrical shell. R_1 is the inner radius, R_2 is the outer radius (both measured in units of 10^{11} cm), h is the height, and τ_o is the total optical thickness in the radial direction. The pure period is 1.24 sec.

R_1	R_2	h/R_2	τ_o	F_p
1.0	2.0	0.5	1.0	0.78±0.053
1.0	2.0	0.5	1.5	0.68±0.042
1.0	2.0	1.0	1.0	0.58±0.027
1.0	2.0	1.0	1.5	0.44±0.019

References

Apparao, K. M. V., 1985, Ap. J., 292, 257.

Bignami, G. F., Maraschi, L. and Treves, A., 1977, Astron. Astrophys., 55, 155.

Boynton, P. E., Crosa, L. M. and Deeter, J. E., 1980, Ap. J., 237, 169.

Chadwick, P. M. et al., 1985, Nature, 318, 642.

Charles, P. A. et al., 1983, M.N.R.A.S., 202, 657.

Crosa, L. and Boynton, P. E., 1980, Ap. J., 235, 999.

Dil Vrtilek et al., 1984, Bull. Am. Astr. Soc., 16, 471.

Elsner, R. F. et al., 1980, Ap. J., 239, 335.

Fechner, W. B. and Joss, P. C., 1977, Ap. J. (Letters), 213, L57.

Gaillardetz, R. et al., 1978, IEEE Trans., NS-25, 437.

Giacconi, R. et al., 1973, Ap. J., 184, 227.

Grindlay, J. E. et al., 1980, Ap. J. (Letters), 240, L121.

Hayaka, S., 1981, Publ. Astron. Soc. Japan, 33, 365.

Joss, P. C. et al., 1973, Ap. J., 225, 994.

Kondo, Y., Van Flandern, T. C. and Wolff, C. L., 1983, Ap. J., 273, 716.

Leahy et al., 1983, Ap. J., 266, 160.

Mason, K. O., et al., 1976, Ap. J., 207, 78.

Milgrom, M., 1976, Astron. Astrophys., 51, 215.

Milgrom, M. and Pines, D., 1978, Ap. J., 220, 272.

Naranan, S. et al., 1985, Ap. J., 290, 487.

Ogelman, H., 1984, Presented at the Symposium "X-Ray Astronomy - 84," Bologna, Italy.

Parsignault, D. R. et al., 1972, Nature Phys. Sci., 239, 123.

Skinner, G. K. et al., 1980, Ap. J., 240, 619.

Skinner, G. K. et al., 1982, Nature, 297, 568.

Weisskopf, M. W. et al., 1981, Ap. Letters, 22, 49.

Williams, A. C., Elsner, R. F., Weisskoof, M. C. and Darbro, W., 1984, Ap. J., 276, 691.

Figure Captions

Fig. 1 The geometry showing the paths of an unscattered photon and a photon which travels a distance s before scattering once by an angle a. Both photons are observed by a distant observer.

Fig. 2 The pulsed fraction as a function of the optical thickness assuming a uniform spherical cloud of ionized plasma of radius 10^{12} cm. The two curves correspond to the pulse periods 1.0 sec and 0.01 sec as indicated.

Fig. 3 The pulsed fraction as a function of the optical thickness assuming a uniform spherical shell of ionized plasma with inner radius 0.5×10^{12} cm and outer radius 10^{12} cm. The two curves correspond to the pulse periods 1.0 sec and 0.069 sec as indicated.

Fig. 4 The observed pulsed fraction as a function of intensity for the source Her X-1.

A. C. Williams and M. C. Weisskopf

Space Science Laboratory
NASA Marshall Space Flight Center
Huntsville, Alabama 35812

K. M. V. Apparao
Space Physics Group
TATA Institute of Fundamental Research
Bombay, India

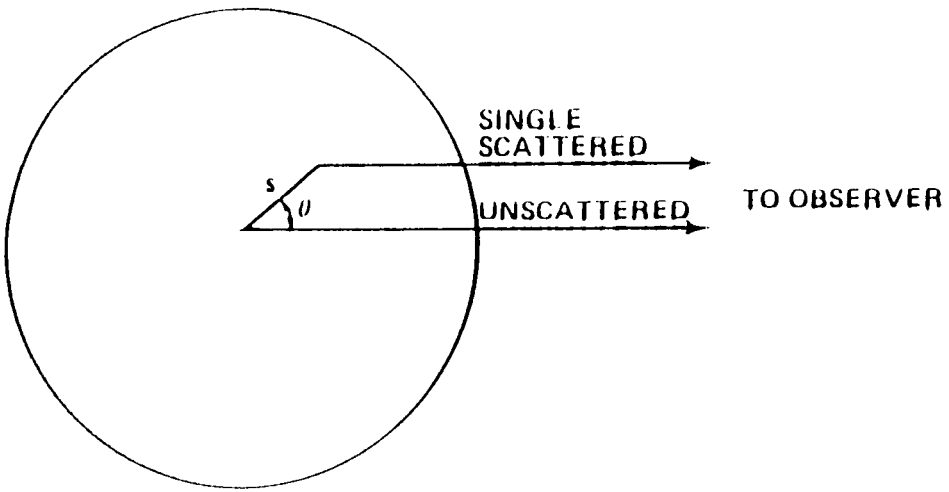

FIG. 1

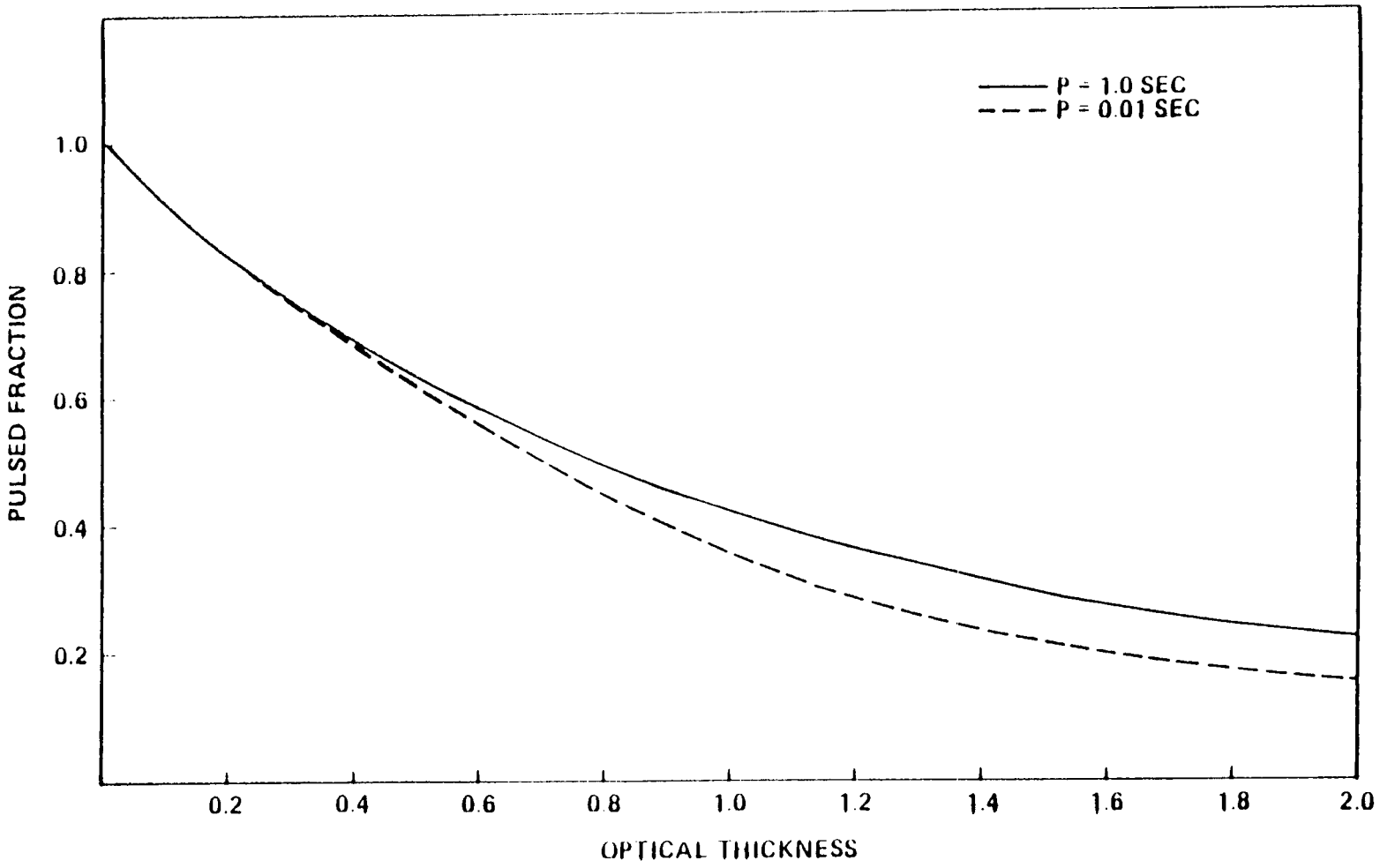
P = 1.0 SEC
P = 0.01 SEC
PULSED FRACTION
1.0
0.8
0.6
0.4
0.2
0.2
0.4
0.6
0.8
1.0
1.2
1.4
1.6
1.8
2.0
OPTICAL THICKNESS

FIG. 2

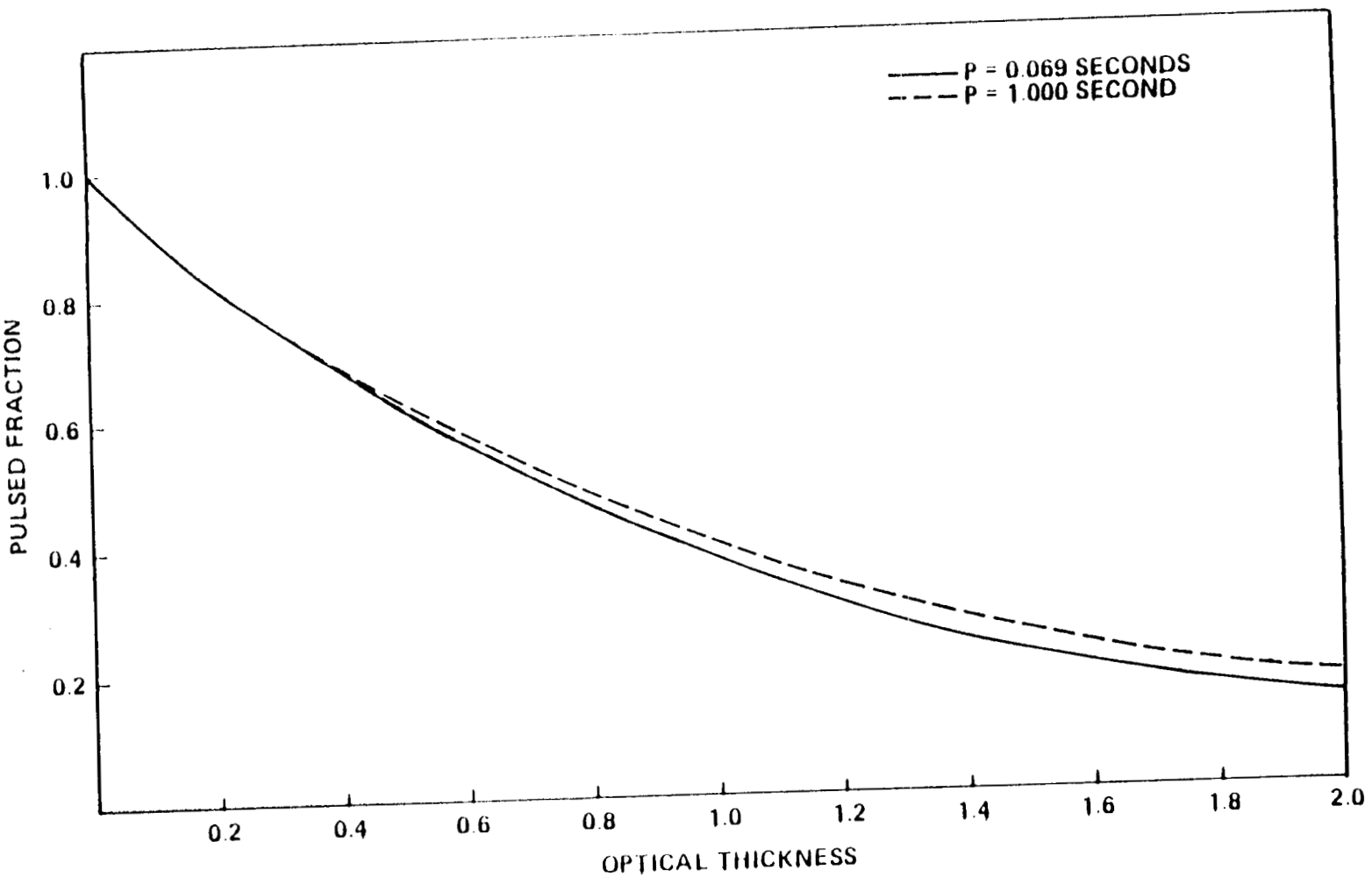
P = 0.069 SECONDS
P = 1.000 SECOND
PULSED FRACTION
1.0
0.8
0.6
0.4
0.2
0.2
0.4
0.6
0.8
1.0
1.2
1.4
1.6
1.8
2.0
OPTICAL THICKNESS

FIG. 3

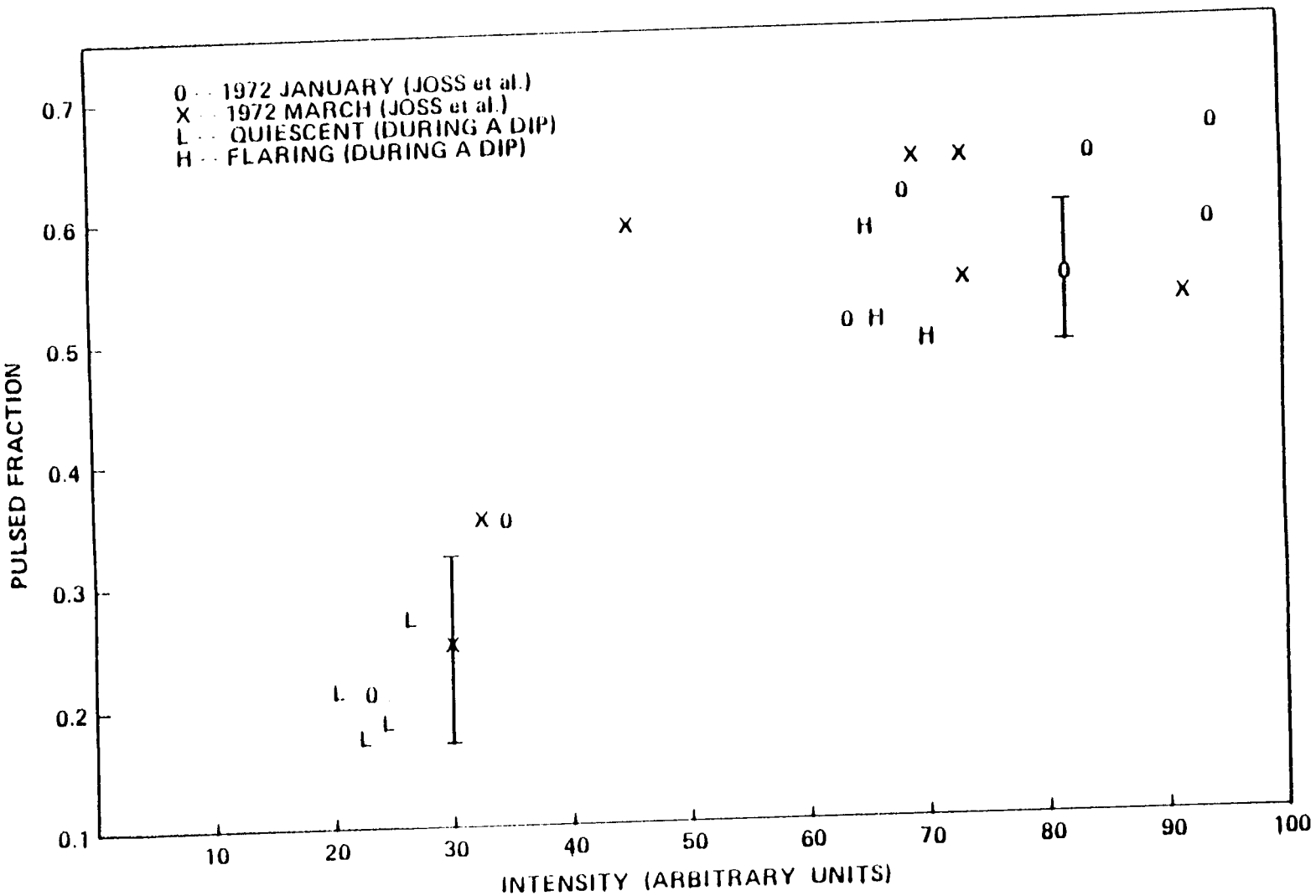
0 - 1972 JANUARY (JOSS et al.)
X - 1972 MARCH (JOSS et al.)
L - QUIESCENT (DURING A DIP)
H - FLARING (DURING A DIP)
PULSED FRACTION
0.7
0.6
0.5
0.4
0.3
0.2
0.1
10
20
30
40
50
60
70
80
90
100
INTENSITY (ARBITRARY UNITS)

FIG. 4